

Article

The Influence of the Cu Foam on the Electrochemical Reduction of Carbon Dioxide

Yuan-Gee Lee ¹, Hui-Hsuan Chiao ², Yu-Ching Weng ^{2,*}  and Chyi-How Lay ^{3,4} 

¹ Department of Automation Engineering, Institute of Mechatronic Systems, Chien-Kuo Institute of Technology, Changhua 50094, Taiwan; yglee@ctu.edu.tw

² Department of Chemical Engineering, Feng Chia University, Taichung 40724, Taiwan; coco6009coco6009@gmail.com

³ General Education Center, Feng Chia University, Taichung 40724, Taiwan; chlay@mail.fcu.edu.tw

⁴ Master's Program of Green Energy Science and Technology, Feng Chia University, Taichung 40724, Taiwan

* Correspondence: ycweng@fcu.edu.tw; Tel.: +886-424517250 (ext. 3689)

Abstract: Unlike the flat Cu sheet, we employed Cu foam to explore the specific porous effect on the expanding specific area. We found that the foam structure is superior to the sheet feature in the specific location from the morphology investigation. In the practical measurement of surface area, we found that the adsorbate could aptly agglomerate, resulting in a consequential block in the transport path. The specific location of the Cu foam was underestimated because the channels of the deep foam layer were blocked by the agglomerated adsorbate. To explore the protonation process of the electro-reduction, we adopted the carbonate electrolyte as the control group in contrast to the experimental group, the bicarbonate electrolyte. In the carbonate electrolyte, the primary intermediate was shown to be CO molecules, as verified using XPS spectra. In the bicarbonate electrolyte, the intermediate CO disappeared; instead, it was hydrogenated as a hydrocarbon intermediate, CHO*. The bicarbonate ion was also found to suppress electrocatalysis in the deep structure of the Cu foam because its high-molecular-weight intermediates accumulated in the diffusion paths. Furthermore, we found a promotion of the oxidation valence on the electrode from Cu₂O to CuO, when the electrode structure transformed from sheet to foam. Cyclic voltammograms demonstrate a succession of electro-reduction consequences: at low reduction potential, hydrogen liberated by the decomposition of water; at elevated reduction potential, formic acid and CO produced; and at high reduction potential, CH₄ and C₂H₄ were formed from −1.4 V to −1.8 V.

Keywords: foam copper; adsorbate agglomeration; hydrocarbon intermediate



Citation: Lee, Y.-G.; Chiao, H.-H.; Weng, Y.-C.; Lay, C.-H. The Influence of the Cu Foam on the Electrochemical Reduction of Carbon Dioxide. *Inorganics* **2024**, *12*, 57. <https://doi.org/10.3390/inorganics12020057>

Academic Editor: Maurizio Peruzzini

Received: 19 December 2023

Revised: 2 February 2024

Accepted: 7 February 2024

Published: 11 February 2024



Copyright: © 2024 by the authors. Licensee MDPI, Basel, Switzerland. This article is an open access article distributed under the terms and conditions of the Creative Commons Attribution (CC BY) license (<https://creativecommons.org/licenses/by/4.0/>).

1. Introduction

Since the Second Industrial Revolution, scientific technology has inspired a new era of innovation and automation, which has consumed vast amounts of fuel and, at the same time, has released a large amount of CO₂ in the atmosphere. The global average atmospheric carbon dioxide concentration has increased from 285 to 419 ppm [1]. The increase in CO₂ concentration promoted the global average surface temperature from 0.97 to 1.21 °C between 1850 and 2022 [2]. Carbon dioxide is a criterion of carbon equivalent for carbon neutrality. It also represents an alternative carbon reservation storage [1,2] for economical fuel recycling, including various MeOH heterocycles and carboxylated structures [3]. Therefore, several research studies have focused on the chemical conversion of CO₂ to obtain available renewable energy sources, of which the ideal conversion would be to convert CO₂ to green derivatives. It not only decreases the amount of carbon but also meets the release requirement of the 17 sustainable development goals, i.e., SDGs. Different technologies were proposed to follow the Sustainable Development Goals, to capture and sequester CO₂ geologically and to convert CO₂ into useful low-carbon fuels [4]. For the latter, CO₂ conversion, it can be achieved by chemical methods [5,6], by photocatalytic and

electrocatalytic reduction [7,8], and by other means [9,10]. Electrochemistry is an effective and economical tool for CO₂ conversion.

The electrochemical reduction of CO₂ produced various products, which depend mainly on the catalyst materials and the reaction medium. In an aqueous solution, three electrocatalytic routes were proposed to reduce CO₂ to formate, to illustrate their mechanisms related to the different intermediates, i.e., *COOH, *OCOH, and *H [11]. Among these three paths, *OCOH is the most favored intermediate [12]. Feaster et al. investigated the strength of the binding energy between the *OCHO intermediate and the metal electrodes. They found that gold, silver, platinum, and copper are weak-binding metals, i.e., weak interaction to form formate, and hence, they show high selectivity. On the contrary, nickel and zinc are strong-binding metals. Adsorbed formate is not expected to desorb quickly from the electrode [12,13]. The copper electrode has unique characteristics, high efficiency, and high selectivity to reduce CO₂ to organics, for example, methane, ethylene, and alcohols, at high current densities, in aqueous electrolytes [14]. In the electrochemical reduction process, CO₂ can proceed with a series of electron charge transfers in gaseous, aqueous, and nonaqueous phases in different cells and electrodes. The main products include carbon monoxide (CO), formic acid (HCOOH) or formate (HCOO), formaldehyde (CHO), methanol (CH₃OH), methane (CH), ethylene (CH-CH), and ethanol (CH₃CH-OH). Among the various chemicals, CH₃OH is one of the highly economical derivatives that exhibits low Faradic efficiency (FE) and therefore a low production [15]. Metal foams with a three-dimensional (3D) porous structure occasionally possess unique properties, such as high specific surface area and structural rigidity. They are suitable self-supported substrates on which active functional groups grow in situ or are coated; in addition, they serve as self-supported current collectors [16]. Cu foam with an integrated 3D pore structure is expected to offer great potential to dramatically improve electrocatalytic performance [17]. This study explored the porous effect on the electrochemical output of the CO₂ reduction reaction (CO₂RR), employing Cu foam as an electrode and comparing it with the Cu sheet electrode. Bicarbonate is a superior electrolyte whose local concentration increases with its bulk concentration, resulting in increased electroreduction activity of CO₂ [18]. Bicarbonate ions could electro-reduce CO with a higher FE value. We adopted carbonate as a contrast electrolyte, by exploring the variation of the reduction mechanism resulting from the intra-hydrogen of the bicarbonate ion.

2. Results and Discussion

The Cu foam prevailed over the Cu sheet in the specific area and in the enrichment of micropores for mass transport. Figure 1 shows the morphology of the Cu sheet and Cu foam. In Figure 1a, the Cu sheet showed a flat feature, enlarged with an irregular pyramidal topography in the inserted picture. On the contrary, a dendritic structure spread throughout the Cu foam with a 200 μm average pore diameter in Figure 1b. The dendritic structure displayed a columnar micropore with interconnected channels. The dendritic structure enriches the surface area, but the interlinked columns serve as self-current collectors to deliver high charge/discharge capacities [19]. Porous channels could provide a fast diffusion path and suppress the change in volume [20]. We conclude that the Cu foam benefited from the high specific area and micropores for the electrocatalytic reaction.

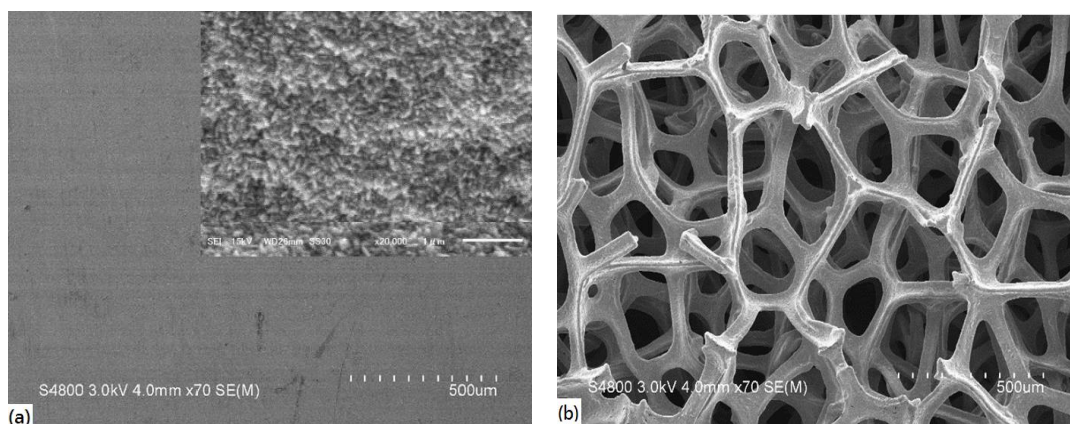


Figure 1. Morphology of the as-received (a) Cu sheet and (b) Cu foam.

The isotherms of the BET test elucidated the adsorption/desorption of the adsorbate. Figure 2a shows the isotherms of the Cu sheet, which showed two maxima in the adsorption process and a maximum in the desorption process, respectively. In the adsorption stage, the adsorbate, i.e., the nitrogen molecule, is randomly adsorbed on the wall of the adsorbent, i.e., Cu grains, initially. With increasing relative pressure, the adsorbate covered the adsorbent. These adsorbates agglomerated with their intrinsic lateral attractive force [21]. The agglomerated mass grew so fast that it filled the crevice, and the cohesive force of the bottom adsorbate could not be maintained at the tolerant compressive pressure [22]. The agglomerated molecules cleared the crevice and spread into the atmosphere from the maximum, as shown in Figure 2a. The Cu sheet was determined to reserve few adsorbates.

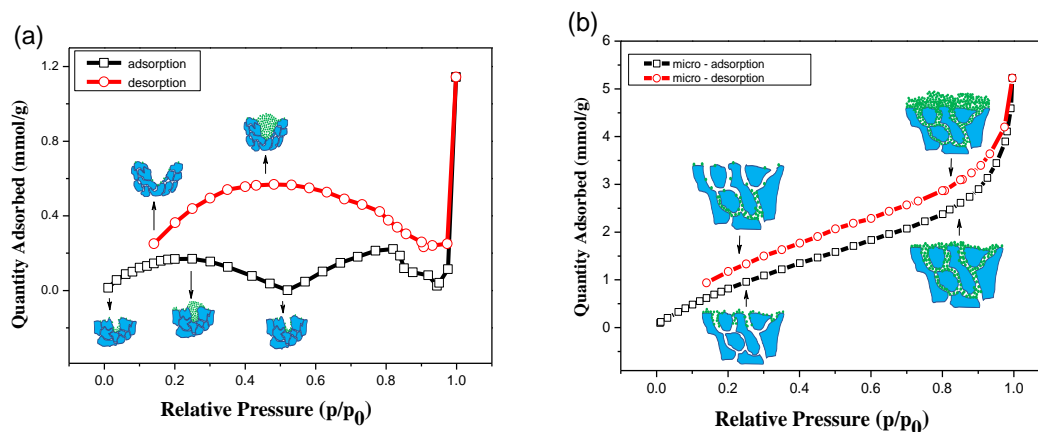


Figure 2. Isothermal absorption and desorption curves for (a) Cu sheet and (b) Cu foam in a N_2 atmosphere.

The dendritic structure could retain the adsorbate but was limited to the shallow layer. Figure 2b shows the isotherms of Cu foam, which showed a convex isotherm and a hysteresis loop. The convex curve, not a steep line, represented an unrestricted multi-layer process in which the adsorbate adsorbed on the columnar wall with non-Langmuir absorption. In this process, the agglomeration filled the columnar channels quickly. Immediately, the lateral agglomeration became an obstacle that hindered the deep channels during micropore filling. In the desorption process, only the nitrogen molecules in the top layer escaped the dendritic layer, with appreciable agglomeration remaining in the deep structure [23]. Therefore, a hysteresis loop was produced on the isotherm with retained adsorbate in the dendritic structure in Figure 2b. The specific area for the Cu sheet and the Cu foam is $0.79 \text{ m}^2/\text{g}$ and $4.76 \text{ m}^2/\text{g}$ and exhibit a 1/6 ratio, which was above the value of the morphology investigation in Figure 1. This is because the area is measured

using the porosimetry analyzer, in which the measurement model was based on Langmuir behavior, i.e., monolayer absorption. The specific area test underestimated the actual value because the foam structure restricted the adsorbate to the shallow layer, leaving a large space underneath the blocked network.

The absorbed CO molecules were verified to be the primary intermediate in the carbonate electrolyte. In contrast, the intermediate was replaced with a hydrocarbon to form a heavy product in the bicarbonate electrolyte. Figure 3 shows the XPS spectra of element O for different electrodes and electrolytes. Notably, the broadening peaks were labeled as O(CO) at ca. 535 eV in Figure 3a,b and appeared with the carbonate electrolyte. These peaks were identified as CO, which was strongly bonded to the electrode as an intermediate on the electrode [24]. These adsorbed CO adsorbates were shown to produce opposite-charged carbon atoms for CO dimerization and form C2 products [25]. In contrast to the carbonate electrolyte, the O(CO) peaks disappeared in Figure 3c,d, in which the carbonate electrolyte was replaced with bicarbonate. The absence of O(CO) peaks indicates an electrolyte effect on the debonding of the absorbed CO on the electrode. This is due to the intra-proton of the bicarbonate ion, which could achieve lower activation energy to saturate the dangling bond of the CO molecule than the proton derived from the decomposed water molecule, as shown in the schematic plot, Figure 4. This proton hydrogenated the absorbed CO to form a hydrocarbon intermediate, CHO^* , with higher molecular weight [26]. Therefore, the absorbed CO molecules were removed from the electrode; thus, molecules with higher molecular weight, e.g., C2 hydrocarbons, formed.

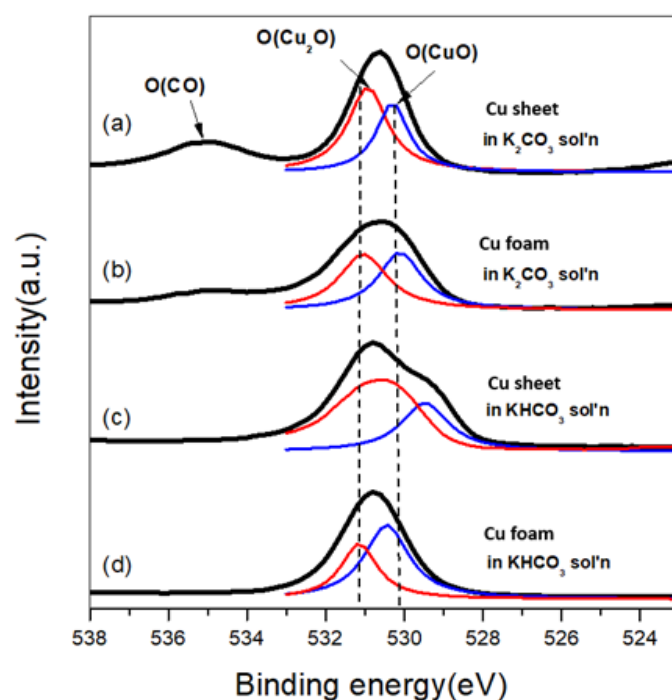


Figure 3. XPS spectra of element O for (a) Cu sheet in K_2CO_3 ; (b) Cu foam in K_2CO_3 ; (c) Cu sheet in KHCO_3 ; and (d) Cu foam in KHCO_3 experiencing a cyclic voltammetry test in which the scan rate was 50 mV/min with an applied potential range from -1.8 V to 0.4 V vs. Ag/AgCl (sat'd). Red and blue lines mean the oxidation states of Cu_2O and CuO, respectively.

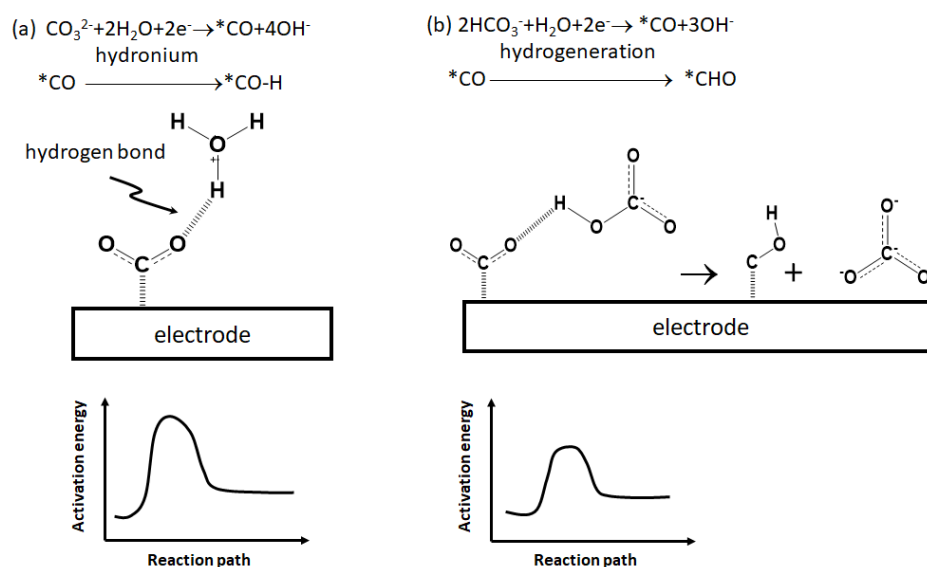


Figure 4. Electrochemical reaction mechanism for the formation of the intermediate in different electrolytes: (a) carbonate and (b) bicarbonate.

The ratio of the peak height of Cu(I) to that of Cu(II) reveals the extent of oxidation on the electrodes. It is due to the asymmetrical feature of the O peak in XPS, which indicates a convolutional peak of different binary oxides, Cu_2O and CuO . We deconvoluted all O (1 s) peaks into two peaks according to specific oxidation, Cu(I) and Cu (II), i.e., Cu_2O and CuO , in Figure 5. The focus is on the top two peaks, in Figure 5a,b, which used the same electrolyte, K_2CO_3 on different electrodes; the peak area ratio of Cu_2O to CuO decreased from Cu sheet to Cu foam. This decrease in the ratio qualitatively represents a decrease in the phase ratio of Cu_2O to CuO , i.e., Cu (I)/Cu (II). A similar trend was also found in different electrolytes in Figure 5c,d, in which bicarbonate was used as the electrolyte. This decrease in the peak height ratio suggests a promotion of the oxidation valence from Cu_2O to CuO , when the electrode structure transformed from sheet to foam. It is due to the per-oxidized Cu electrode, which is known to promote C2 products [27,28]. Thus, we briefly concluded that not only the foam structure but also the bicarbonate electrolyte could facilitate oxidation on the electrode.

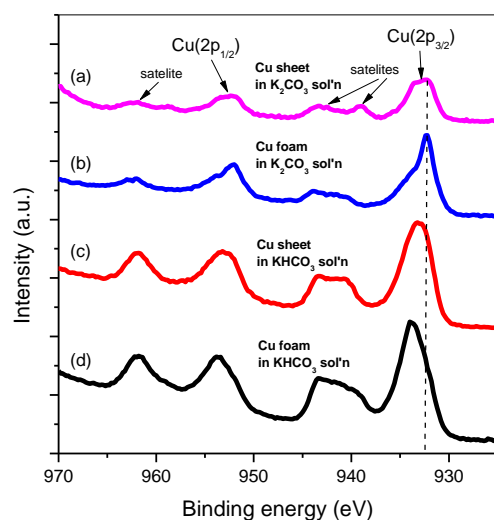


Figure 5. XPS spectra of the element Cu for (a) Cu sheet in K_2CO_3 ; (b) Cu foam in K_2CO_3 ; (c) Cu sheet in KHCO_3 ; and (d) Cu foam in KHCO_3 that underwent a cyclic voltammetry test in which the scan rate was 50 mV/min with an applied potential range of -1.8 V to 0.4 V vs. Ag/AgCl (sat'd).

Nevertheless, Dutta and his coworkers investigated the stability of Cu⁺ ions using skeleton-type Cu catalysts. They found that the sample modified with Cu foam showed profound activities towards the C₂ products, C₂H₄ and C₂H₆, with Faradic efficiency, FE_{C₂H₄} = 32.3%, whereas the Cu skeleton without foam remained largely inactive for the C₁ and the C₂ products of hydrocarbon [29]. They attributed this effect to the residual impurities left behind from the casting approach process on which the fabrication of these Cu skeleton support materials is based. Furthermore, the absence of Cu⁺ in Cu grains could change the selectivity of the C₂H₄ reaction to CH₄. They approved that highly porous 3D Cu dendrites and foam exhibited excellent CO₂RR with improved C₂H₄ selectivity [29,30]. They concluded the priority for selectivity, i.e., the first is superior facet reorientation in nanostructured materials, and the next is high-density defects (steps, kinks, and edges) [31], grain boundaries [32] and surface roughness [30,31], and concurrent changes in the interfacial pH [33], regarded as critical considerations outlining the subsequent catalytic behaviors. Furthermore, the stability of the intermediates within the 3D catalysts is crucial for the selectivity of the C₂ product.

Cyclic voltammograms (CV) and Faradic efficiency revealed the reaction sequence and mechanism. Figure 6a,b show the cyclic voltammograms of Cu sheet and Cu foam electrodes in a 0.5 M Na₂CO₃ electrolyte under N₂ and CO₂ atmospheres. In Figure 6a, in the absence of CO₂, the Cu sheet electrode exhibits two oxidation peaks at −0.204 and −0.015 V vs. Ag/AgCl, indicating the oxidation of Cu to CuO and Cu₂O. Two reduction peaks at −0.277 and −0.716 V vs. Ag/AgCl represent the reduction of CuO and Cu₂O to Cu. At more negative potentials than −1.143 V vs. Ag/AgCl, a rapid increase in the current indicates the occurrence of the hydrogen evolution reaction. In the presence of CO₂, the oxidation and reduction peaks of Cu are influenced by CO₂ adsorption on the electrode surface. The reduction reaction of CO₂ begins at −1.058 V vs. Ag/AgCl, preceding the hydrogen evolution reaction. In contrast to the Cu sheet electrode in the absence of CO₂, the Cu foam electrode requires a more positive potential to oxidize Cu, as shown in Figure 6b. The Cu foam electrode also exhibits two reduction peaks, representing the reduction of CuO and Cu₂O to Cu. In the presence of CO₂, the Cu foam electrode catalyzes the reduction of CO₂ at a more positive potential than the hydrogen evolution potential. Furthermore, the catalytic reduction current for CO₂ is significantly higher for the Cu foam electrode than for the Cu sheet electrode.

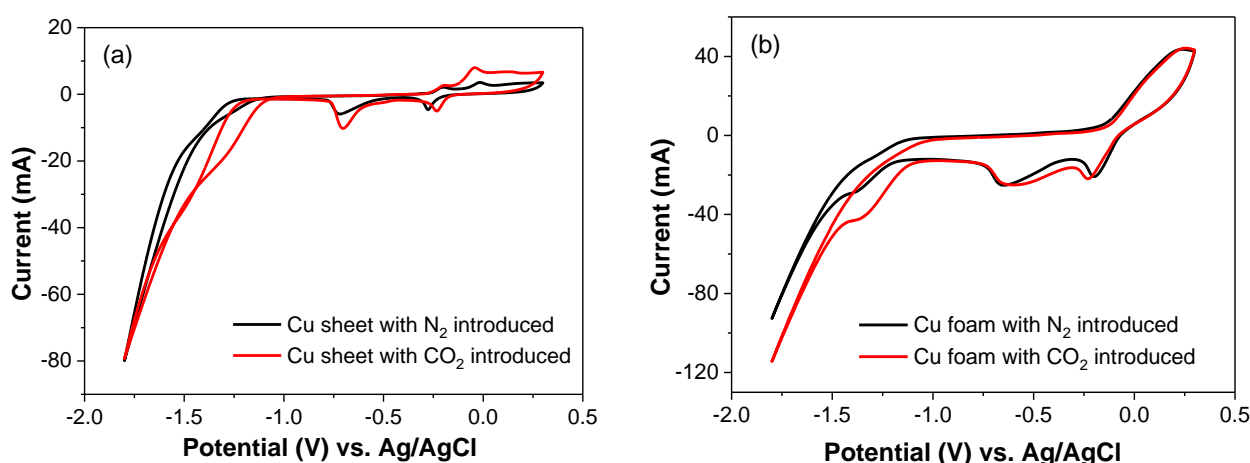


Figure 6. Cyclic voltammograms of (a) Cu sheet and (b) Cu foam electrodes, in which the electrolyte was 0.5 M K₂CO₃ at 0.3 V to −1.8 V vs. Ag/AgCl potential; the scan rate was 100 mV/s; and the gas was introduced with N₂ and CO₂.

The products of CO₂ reduction reaction were qualitatively identified and quantitatively transferred to Faradic efficiency, as shown in Figure 7. In Figure 7, H₂ dominated at all potentials and increased with decreasing reduction potential. Inversely, in contrast, CH₄

decreased with increasing reduction potential. This indicates a succession of reduction consequences, i.e., at low reduction potential, -1.0 V, the current contributed mainly to the decomposition of water molecules with hydronium left. As soon as these hydroniums approached the electrode, the hydrogen molecule, H_2 , was synthesized and escaped from the electrode. The rest of the hydroniums remained on the dehydrated electrode, leaving protons for hydrogen transfer with the on-site carbon-rich atoms. As the reduction potential was elevated, more CO was produced by decomposing CO_2 gas through a heterogenic reaction [34]. Some of the CO molecules escaped to the atmosphere; the rest of the CO received protons and transformed to CHO, a significant intermediate, and then formed formic acid, HCOOH, at potentials from -1.1 V to -1.4 V. With a higher increase in the reduction potential from -1.4 V to -1.8 V, the precursor proceeded to an exergonic reaction to produce CH_4 and C_2H_4 that were synthesized with the adsorbed intermediate species on the electrode [15]. Notably, CH_4 showed the highest FE value at -1.8 V, when the sheet electrode was replaced with the foam electrode from Figure 7a to Figure 7b and from Figure 7c to Figure 7d. Compared to the previous result in Figure 4, the decrease in the phase ratio of Cu(I)/Cu(II) from Cu sheet to Cu foam matches Dutta's conclusion that Cu^+ on Cu grains could shift the selectivity of the C_2H_4 reaction to CH_4 .

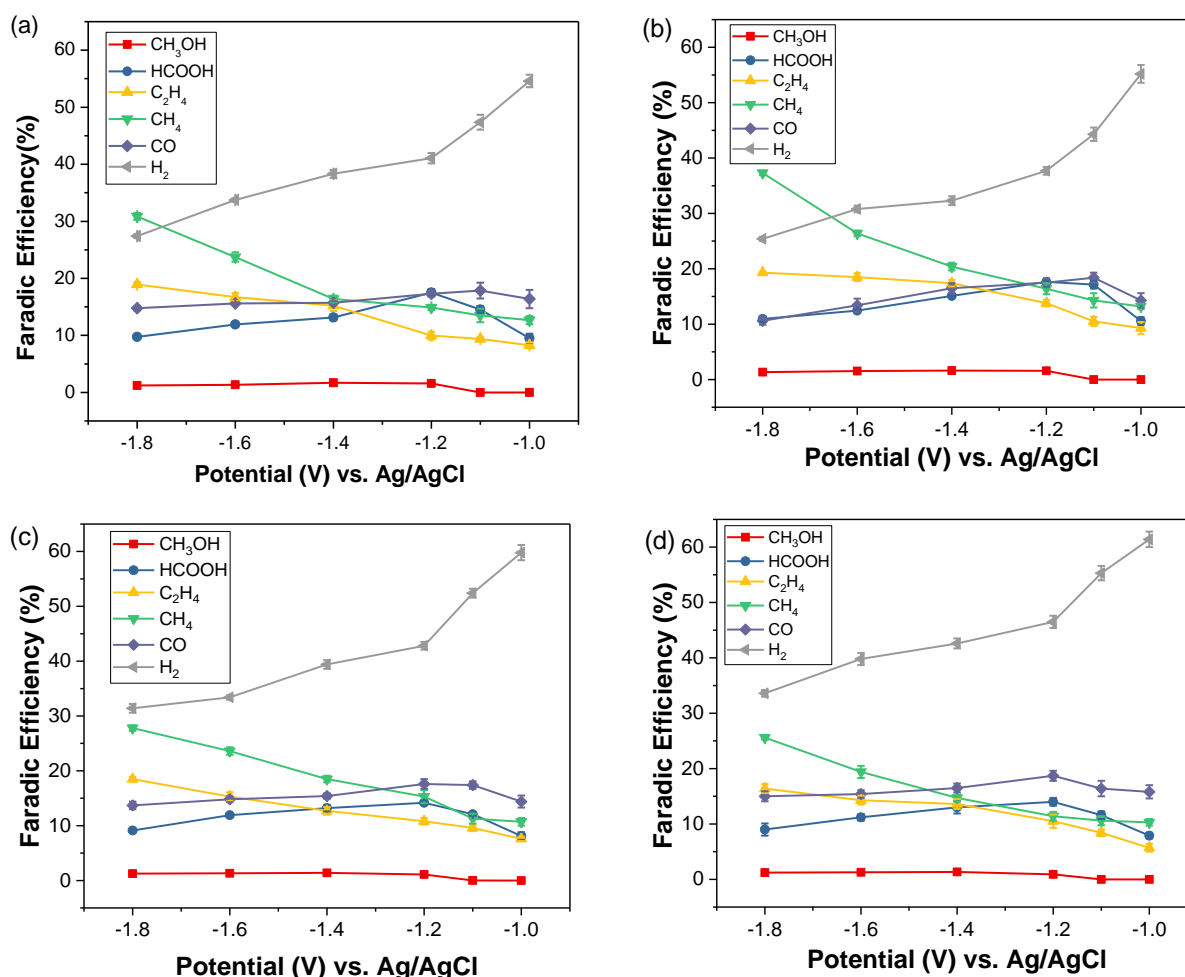


Figure 7. Faradic efficiency for the different electrodes: (a) Cu sheet; (b) Cu foam, in 0.5 M K_2CO_3 electrolyte; (c) Cu sheet; and (d) Cu foam, in 0.5 M $KHCO_3$ electrolyte.

It is necessary to tabulate the results obtained for the Cu-based foam structure [35–44] for comparison and are shown in Table 1. In particular, the economical product, ethene, is selected as the criterion in the table to evaluate the FE of CO_2RR . In Table 1, almost all FE values are less than 50%, except for nano-deposited Cu dendrites and nano-porous

CuAg alloy electrodes [30,41]. In addition, all electrodes with a nano-scaled microstructure, e.g., nanoporous Cu films, nano-deposited Cu dendrites, nano-porous CuAg alloy, porous-Cu nanoribbons, and nanoporous Cu films, possessed high FE values of more than 40% [37,39,41,43]. On the contrary, the FE value is 9.6%, although the electrode in this study possessed a foam surface with a pore size, 200 μm , mentioned in the previous paragraph.

Table 1. Faradic efficiency (FE) of ethylene (C_2H_4) produced by different porous metal electrodes in the electroreduction of CO_2 .

Electrode	FE (%)	Electrolyte	E (vs. RHE)	Current Density (mA/cm ²)	Ref
Ag ₁₅ Cu ₈₅ foam	36	0.5 M KHCO ₃	−1.1	−11.32	[35]
Cu _x O foam	6	0.5 M KHCO ₃	−0.67	0.47	[36]
Nanoporous Cu films	46	0.1 M KHCO ₃	0.96	14.3	[37]
Ag (CO)	5	0.5 M KHCO ₃	−1.5	−36	[38]
Cu (C2 hydrocarbons)	22	0.1 M KHCO ₃	−0.8	−12	[30]
Nano-deposited Cu dendrites	57	0.1 M KBr/Br ₂	−1.85	170	[39]
Porous Cu films	34.8	0.1 M KHCO ₃		18	[40]
Nano-porous CuAg alloy	60	1 M KOH	−0.7	300	[41]
Poly-amide-modified Cu foam	26	0.10 M NaHCO ₃	−0.95	110	[42]
Nanoporous Cu films	40	1 M KOH		700 A/g	[43]
Cu foam	9.6	0.5 M KHCO ₃	−0.9	5.6	This study

Note: the potential conversion between RHE and Ag/AgCl sat. was calculated using the following formula: $E(\text{RHE}) = 197 \text{ mV} + E(\text{Ag}/\text{AgCl}) + 0.059 \text{ pH}$.

The bicarbonate ion could suppress the electrocatalysis in the deep structure of the Cu foam. Figure 8a showed the dependence of the response current vs. the scan rate in the 0.5 M carbonate ion. Both the Cu sheet and the Cu foam showed a steep linear relationship in which the large slope suggests a reaction-controlled mechanism. Notably, the Cu foam benefited from its high specific area, to show a slope three times that of the Cu sheet. In contrast to the carbonate electrolyte, the dependence of the response current versus the square root of the scan rate in 0.5 M of bicarbonate ion is observed in Figure 8b. The Cu sheet and the Cu foam showed a pair of parallel-like linear relationships, suggesting a diffusion-controlled mechanism in the scan rate of less than 200 mV/sec. In addition, these parallel lines demonstrate a constant active-site ratio of Cu foam to Cu sheet. Particularly, these two linear curves turned flat and even overlapped in height scan rate. The slope inflection elucidates a transition of mass transport for the long-chained intermediate. It is due to the intra-proton in carbonate ion, which could convert CO to an intermediate with high molecular weight, as shown in Figure 4. Although the Cu foam due to its advantageous high specific area performed better than the Cu sheet in terms of the response current, the long-chained intermediate in the deep foam structure could not compete with the diffusion rate at a high scan rate. This long-chained intermediate blocked the diffusion channels. This was confirmed by Abhijit and his co-workers' research, in which they investigated the dependence of the size of the morphology by tuning the pore size of the Cu oxide-derived foam in CO_2 electroreduction [30]. They found that the FE reached its maximum, i.e., 55%, when the pore size was between 50 μm and 100 μm . Beyond the size range, the FE decreased dramatically. In contrast to this study, the ratio of the normalized specific area for Cu foam to Cu sheet is 0.79/17.57, i.e., 22, see Section 3.3; however, the current density ratio of the Cu foam to the Cu sheet was ca. 4 in Figure 8a, 0.5 M K_2CO_3 , or Figure 8b, 0.5 M KHCO₃. The latter ratio is far less than the former ratio, which suggests that a mass diffusion barrier, i.e., intermediate, blocked in the foam structure to induce a diffusion-controlled mechanism. Only the sites on the surface were still involved in electrocatalysis, with inert active sites remaining in the deep foam. Therefore, we conclude that the reduction reaction was suppressed when the electrolyte was switched from carbonate to bicarbonate.

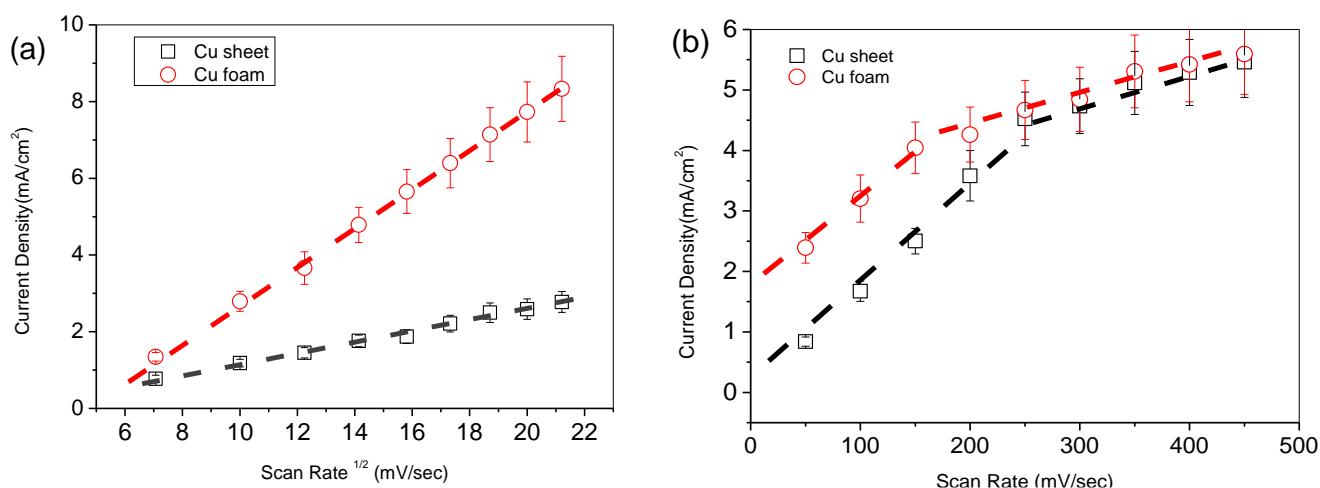


Figure 8. Response current vs. scan rate for different electrolytes: (a) 0.5 M K₂CO₃ and (b) 0.5 M KHCO₃.

3. Materials and Methods

3.1. Preparation of the Electrodes

The Cu foam and the Cu sheet were used as the working electrodes (WE). Commercially available Cu foam and Cu sheet (May Chun Co., Taichung, Taiwan) were purchased as experimental and control groups. They were cut into small slices with a dimension of 1.25 cm × 2.5 cm × 0.1 cm. The Cu foam slices were ground with abrasive paper grit 500 to 2000; in contrast, the Cu sheets were ground and polished with grit 2000 of abrasive paper. They were cleaned ultrasonically in a batch containing acetone for 10 min and then in deionized (DI) water for 10 min successively. These slices were dried in a vacuum oven at 60 °C for 1 h. Among the polished Cu sheets, one with a dimension of 2.5 cm × 5.0 cm × 0.1 cm was used as a counter electrode (CE). In an aqueous solution, all potentials were specified for the Ag/AgCl/saturated reference electrode (RE-1s Bio-Logic Co., Seyssinet-Pariset, France). The electrochemical system is shown in Figure 9.

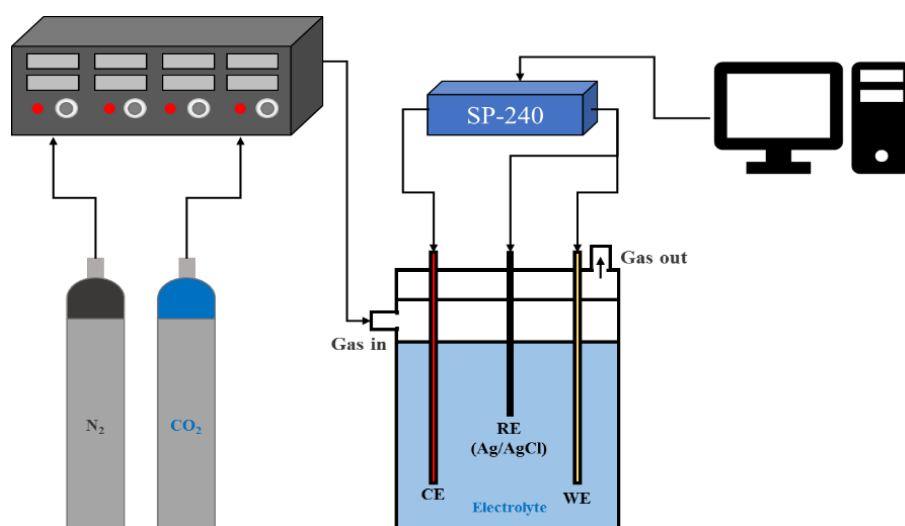


Figure 9. Electrochemical system for CO₂ reduction.

It is due to the uncompensated resistance, R_u , which could result from overestimating the applied potential between the working electrode (WE) and the reference electrode (RE). To minimize the impact of the iR drop, we primarily reduced both the currents (i) and the resistance (R_u) between the WE and RE. For the former, the WE areas were designed by

trial and error to reduce the current to less than 10 mA; for the latter, the distance between the WE and the RE was minimized. In addition, we checked with the potentiostat supplier who confirmed that the iR compensation module works by the means of positive feedback.

3.2. Preparation of the Electrolysis Batch

The sodium bicarbonate, KHCO_3 , was adopted as the electrolyte of the experimental group due to its high selectivity for CO_2 reduction, while the sodium carbonate, K_2CO_3 , was used as the control group [44]. Carbonate and bicarbonate electrolytes were prepared by weighting 6.36 g of sodium carbonate and 5.04 g of sodium bicarbonate (Alfa Aesar Co.) to dissolve in 60 mL of DI water to obtain a 0.5 M solution. These two electrolytes were used to match alternatively with the two different electrodes, the Cu foam and the Cu sheet. The CO_2 solution was prepared in a batch as follows. Nitrogen gas (Toyogas Co., Taichung, Taiwan), N_2 , was introduced with a mass flow controller (5850E Brooks Co., Hsinchu City, Taiwan) to maintain a rate of 200 mL/min to activate the electrode. The supply of N_2 was turned off; instead, CO_2 gas (Toyogas Co., Taichung, Taiwan) with a flow rate of 200 mL/min was introduced to expel the remaining N_2 gas. Until the increase in CO_2 formed a gas film for 20 min, the solubility of CO_2 was confirmed to be 0.1366 mg per 100 mL of solution. Electrochemical modes were performed with a potentiostat (SP 240 BioLogic Co., Seyssinet-Pariset, France).

3.3. Measurement Equipment for Electrochemical Reaction

The morphology of the electrode was investigated with a scanning electron microscope (SEM, S4810, Hitachi Co., Tokyo, Japan). The specific areas of the Cu sheet and the Cu foam were measured using a high-resolution surface area and porosimetry analyzer (2460 Micromeritics Co., Norcross, GA, USA). The real specific area was evaluated as follows. To ensure the electrochemical reaction limit of the Cu foam, experienced foam was ground from the top side to the bottom side using 1000# abrasive paper. When grinding was completed, the top side of the sample was analyzed using IR spectroscopy until the major peak, C-H, disappeared in the spectrum. Therefore, the reaction depth of the foam was determined, c.a. 0.4 mm, and the "active real weight" of the Cu foam was determined. Then, the "real specific surface" of the foam was evaluated as $17.57 \text{ m}^2/\text{g}$. The binding energy of the electrodes was detected with an X-ray photoelectron spectroscope (XPS, PHI 5000 ULVAC-PHI Co., Kanagawa, Japan). Notably, the samples for SEM and XPS were prepared separately because the sample used for SEM could accumulate carbon on its surface. This implies that the SEM was a destructive testing compared to the XPS test. We designed the Cu sheet and the Cu foam as the experimental group and the control group; on the other hand, we employed the carbonate electrolyte and the bicarbonate electrolyte as the experimental group and the control group, respectively. The XPS analysis was conducted after the electrochemical experiments were completed. The electrodes were dried before performing the XPS analysis.

Qualitative and quantitative measurements of the liquid product, i.e., formic acid (HCOOH), were performed with high-performance liquid chromatography (HPLC, RID-10A, Shimadzu Co., Tokyo, Japan). One microliter of the solution was subjected to the chronoamperometric test and was filtered and then injected into the HPLC. The calibration curve for HCOOH was constructed and is depicted in Figure 10. On the contrary, the gaseous product was measured with gas chromatography. The methanol was detected with a flame ionization detector (GC-FID, GC-2014, Shimadzu Co., Tokyo, Japan); its calibration curve is shown in Figure 11. The other major gaseous products, H_2 , CO , CH_4 , and C_2H_4 , were measured with a thermal conductive detector (GC-TCD, GC-1000, Shimadzu Co., Tokyo, Japan); their calibration curves are shown in Figure 12. All products were evaluated using the Faradic efficiency, i.e., moles of electrons consumed by the specific product per mole of electrons passing through the electrode.

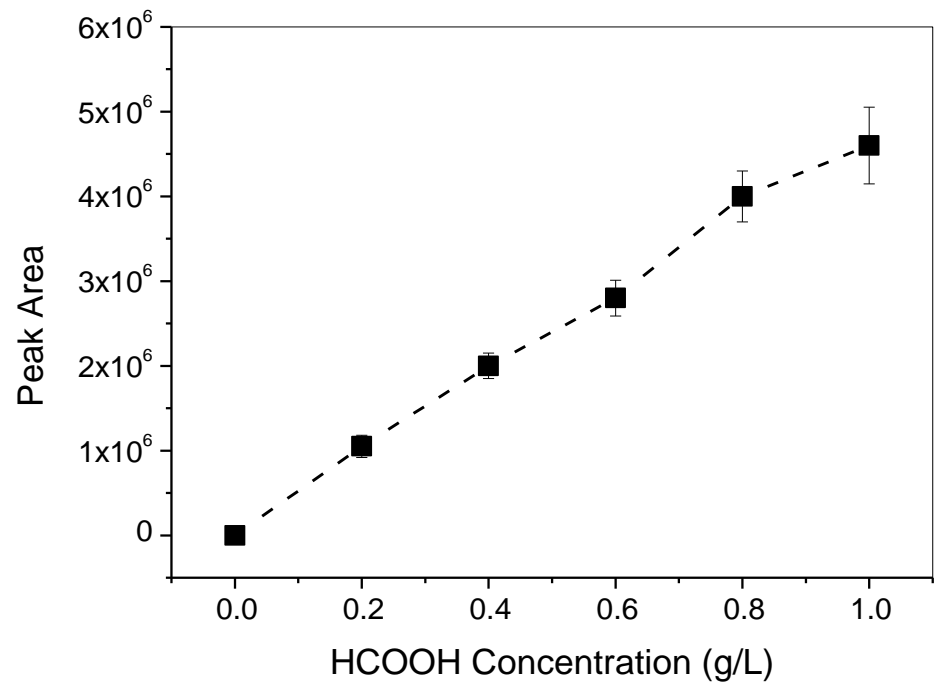


Figure 10. HPLC calibration curve for the liquid product, HCOOH.

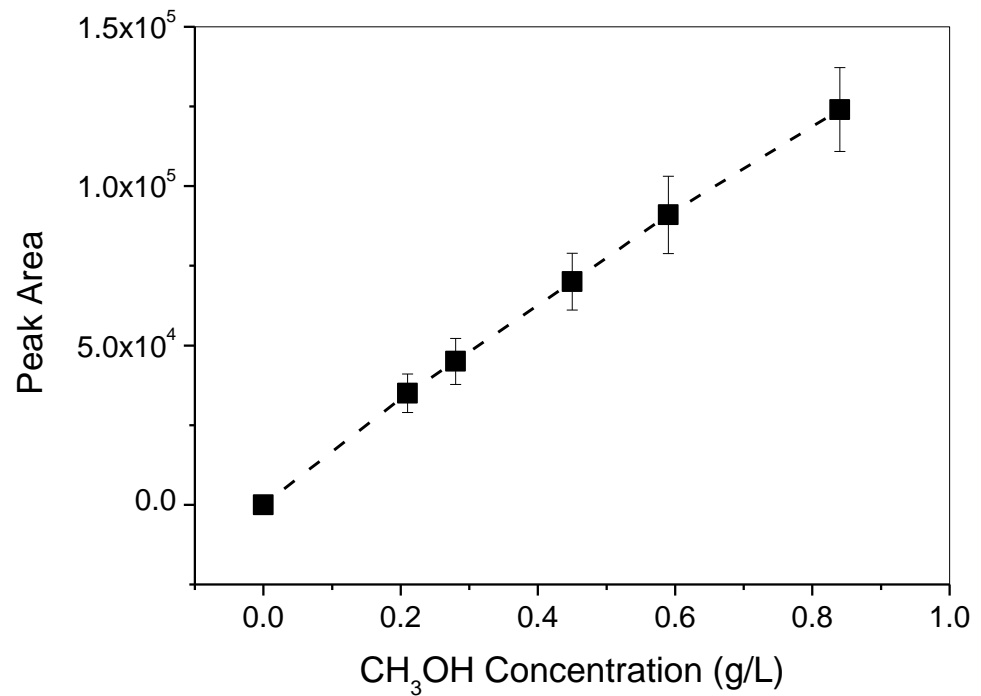


Figure 11. GC-FID calibration curve for the gaseous product, CH₃OH.

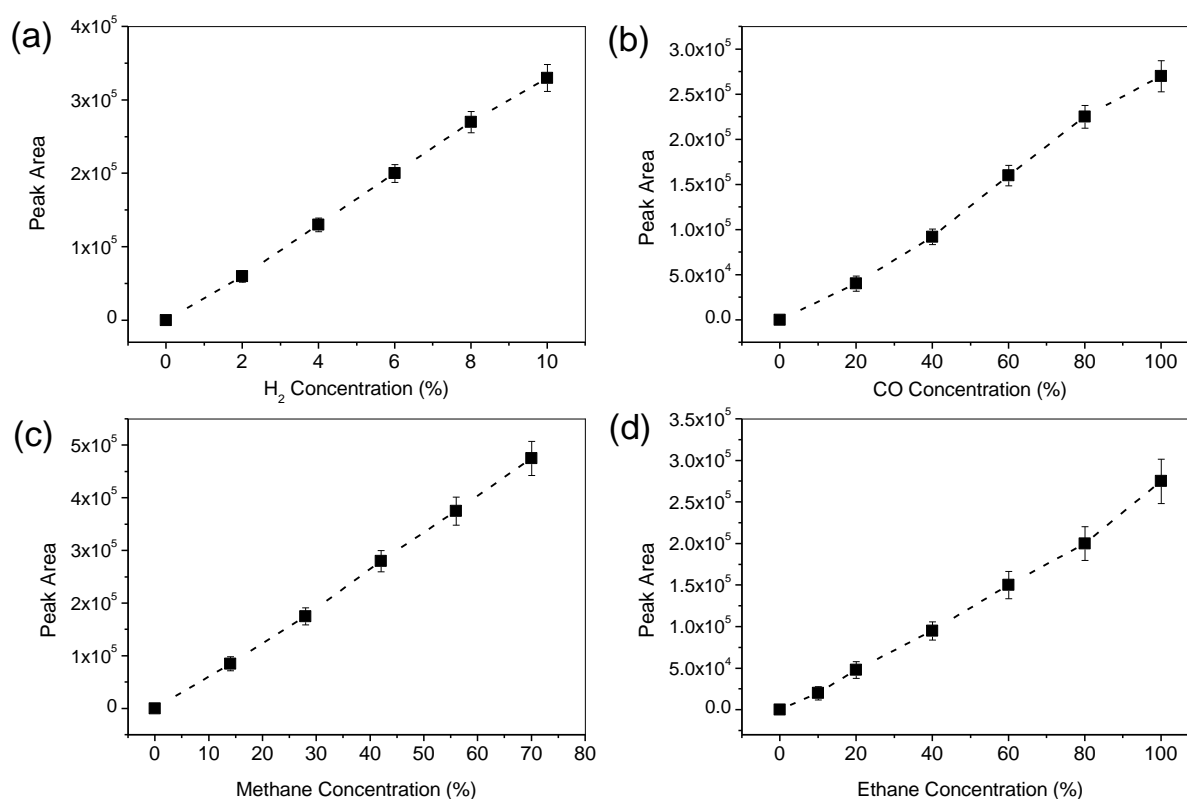


Figure 12. GC-TCD calibration curves for gaseous products: (a) H_2 , (b) CO, (c) CH_4 , and (d) C_2H_4 .

4. Conclusions

From the morphology investigation, the foam structure is superior to the sheet feature in terms of the specific area. In the isotherm, we found that the adsorbate was appropriately agglomerated; the agglomeration blocked the consequential adsorbate. The measured specific area ratio of the Cu sheet to the Cu foam was 1/6, far from the value estimated by the morphology investigation. We employed carbonate in contrast to the bicarbonate electrolyte, to explore the effect of the intra-proton of the bicarbonate ion on the reaction mechanism. In carbonate electrolytes, the XPS spectra identified the primary intermediate as CO molecules. In contrast to the carbonate electrolyte, the CO molecules disappeared; the absorbed CO proceeded to hydrogenate, forming a hydrocarbon intermediate, CHO^* , in the bicarbonate electrolyte. This intermediate induced by the bicarbonate ion was also found to suppress the electrocatalysis in the deep structure of the foam Cu because it had a high molecular weight, with a long chain to block the diffusion paths. In addition, we investigated the phase transformation of the electrode by the peak height ratio of Cu(I) to Cu(II). We found a promotion of the oxidation valence from Cu_2O to CuO, when the electrode structure transformed from sheet to foam. Cyclic voltammograms demonstrate a succession of electro-reduction consequences: at low reduction potential, less than -1.0 V, hydrogen was liberated by the decomposition of water; at elevated reduction potential, formic acid and CO were produced; and at high reduction potential, CH_4 and C_2H_4 were formed from -1.4 V to -1.8 V.

Author Contributions: Conceptualization, Y.-C.W. and Y.-G.L.; methodology, H.-H.C.; validation, Y.-G.L.; formal analysis, H.-H.C.; investigation, H.-H.C., Y.-G.L. and C.-H.L.; resources, Y.-C.W.; writing—original draft preparation, Y.-G.L.; writing—review and editing, Y.-C.W.; visualization, Y.-G.L.; supervision, Y.-C.W.; project administration, Y.-C.W.; funding acquisition, Y.-C.W. All authors have read and agreed to the published version of the manuscript.

Funding: This research was funded by the National Science and Technology Council (grant number: MOST109-2221-E-035-024-MY3).

Data Availability Statement: Data are contained within the article.

Acknowledgments: The authors gratefully acknowledge the support of Feng Chia University and the Precision Instrument Support Center of Feng Chia University, for providing measurement facilities.

Conflicts of Interest: The authors declare no conflicts of interest.

References

1. Chen, J.M. Carbon Neutrality: Toward a Sustainable Future. *Innovation* **2021**, *2*, 100127. [[CrossRef](#)]
2. Chen, L.; Msigwa, G.; Yang, M.; Osman, A.I.; Fawzy, S.; Rooney, D.W.; Yap, P.-S. Strategies to Achieve a Carbon Neutral Society: A Review. *Environ. Chem. Lett.* **2022**, *20*, 2277–2310. [[CrossRef](#)]
3. Centi, G.; Perathoner, S. Opportunities and Prospects in the Chemical Recycling of Carbon Dioxide to Fuels. *Catal. Today* **2009**, *148*, 191–205. [[CrossRef](#)]
4. Saravanan, A.; Kumar, P.S.; Vo, D.V.N.; Jeevanantham, S.; Bhuvanewari, V.; Narayanan, V.A.; Yaashikaa, P.R.; Swetha, S.; Reshma, B. A comprehensive review on different approaches for CO₂ utilization and conversion pathways. *Chem. Eng. Sci.* **2021**, *236*, 8. [[CrossRef](#)]
5. Meyer, T.J. Chemical approaches to artificial photosynthesis. *Acc. Chem. Res.* **1989**, *22*, 163–170. [[CrossRef](#)]
6. Leitner, W. The coordination chemistry of carbon dioxide and its relevance for catalysis: A critical survey. *Coord. Chem. Rev.* **1996**, *153*, 257–284. [[CrossRef](#)]
7. Sakakura, T.; Choi, J.C.; Yasuda, H. Transformation of Carbon Dioxide. *Chem. Rev.* **2007**, *107*, 2365–2387. [[CrossRef](#)]
8. Oloman, C.; Li, H. Electrochemical Processing of Carbon Dioxide. *ChemSusChem* **2008**, *1*, 385–391. [[CrossRef](#)]
9. Thakur, I.S.; Kumar, M.; Varjani, S.J.; Wu, Y.; Gnansounou, E.; Ravindrane, S. Sequestration and utilization of carbon dioxide by chemical and biological methods for biofuels and biomaterials by chemoautotrophs: Opportunities and challenges. *Bioresour. Technol.* **2018**, *256*, 478. [[CrossRef](#)]
10. Roy, S.; Cherevotan, A.; Peter, S.C. Thermochemical CO₂ Hydrogenation to Single Carbon Products: Scientific and Technological Challenges. *ACS Energy Lett.* **2018**, *3*, 1938–1966. [[CrossRef](#)]
11. Koh, J.H.; Won, D.H.; Eom, T.; Kim, N.-K.; Jung, K.D.; Kim, H.; Hwang, Y.J.; Min, B.K. Facile CO₂ electro-reduction to formate via oxygen bidentate intermediate stabilized by high-index planes of Bi dendrite catalyst. *ACS Catal.* **2017**, *7*, 5071–5077. [[CrossRef](#)]
12. Al-Tamreh, S.A.; Ibrahim, M.H.; El-Naas, M.H.; Vaes, J.; Pant, D.; Benamor, A.; Amhamed, A. Electroreduction of Carbon Dioxide into Formate: A Comprehensive Review. *ChemElectroChem* **2021**, *8*, 3207–3222. [[CrossRef](#)]
13. Feaster, J.T.; Shi, C.; Cave, E.R.; Hatsukade, T.; Abram, D.N.; Kuhl, K.P.; Hahn, C.; Nørskov, J.K.; Jaramillo, T.F. Understanding selectivity for the electrochemical reduction of carbon dioxide to formic acid and carbon monoxide on metal electrodes. *ACS Catal.* **2017**, *7*, 4822–4827. [[CrossRef](#)]
14. Hori, Y.; Kikuchi, K.; Suzuki, S. Production of Co and CH₄ in Electrochemical Reduction of CO₂ at Metal Electrodes in Aqueous Hydrogencarbonate Solution. *Chem. Lett.* **1985**, *14*, 1695–1698. [[CrossRef](#)]
15. Hori, Y.; Takahashi, R.; Yoshinami, Y.; Murata, A. Electrochemical Reduction of CO at a Copper Electrode. *J. Phys. Chem. B* **1997**, *101*, 7075–7081. [[CrossRef](#)]
16. Shi, Y.; Wang, Z.; Gao, H.; Niu, J.; Ma, W.; Qin, J.; Peng, Z.; Zhang, Z. A Self-Supported, Three-Dimensional Porous Copper Film as a Current Collector for Advanced Lithium Metal Batteries. *J. Mater. Chem. A* **2019**, *7*, 1092–1098. [[CrossRef](#)]
17. Guo, N.; Xue, H.; Bao, A.; Wang, Z.; Sun, J.; Song, T.; Ge, X.; Zhang, W.; Huang, K.; He, F.; et al. Achieving Superior Electrocatalytic Performance by Surface Copper Vacancy Defects during Electrochemical Etching Process. *Angew. Chem. Int. Ed.* **2020**, *59*, 13778–13784. [[CrossRef](#)]
18. Deng, W.; Yuan, T.; Chen, S.; Li, H.; Hu, C.; Dong, H.; Wu, B.; Wang, T.; Li, J.; Ozin, G.A.; et al. Effect of Bicarbonate on CO₂ Electroreduction over Cathode Catalysts. *Fundam. Res.* **2021**, *1*, 432–438. [[CrossRef](#)]
19. Liu, X.; Yang, Z.; Quan, H.; Li, J.; Xiang, Y.; Wu, F. EGaIn Coated 3D-Cu Foam as a Self-Healing Current Collector for Lithium Ion Batteries. *Electrochem. Commun.* **2021**, *132*, 107145. [[CrossRef](#)]
20. Nesin, O.M.; Pakhomova, O.N.; Xiao, S.; Pakhomov, A.G. Manipulation of Cell Volume and Membrane Pore Comparison Following Single Cell Permeabilization with 60- and 600-Ns Electric Pulses. *Biochim. Et Biophys. Acta (BBA)—Biomembr.* **2011**, *1808*, 792–801. [[CrossRef](#)]
21. Qajar, A.; Peer, M.; Rajagopalan, R.; Liu, Y.; Brown, C.; Foley, H.C. Surface Compression of Light Adsorbates inside Microporous PFA-Derived Carbons. *Carbon* **2013**, *60*, 538–549. [[CrossRef](#)]
22. Kowalczyk, P.; Furmaniak, S.; Gauden, P.; Terzyk, A. Carbon Dioxide Adsorption-Induced Deformation of Microporous Carbons. *J. Phys. Chem. C* **2010**, *114*, 5126–5133. [[CrossRef](#)]
23. Groen, J.C.; Peffer, L.A.A.; Pérez-Ramírez, J. Pore Size Determination in Modified Micro- and Mesoporous Materials. Pitfalls and Limitations in Gas Adsorption Data Analysis. *Mesoporous Mater.* **2003**, *60*, 1–17. [[CrossRef](#)]
24. He, J.; Corneille, J.S.; Estrada, C.A.; Wu, M.; Goodman, D.W. CO Interaction with Ultrathin MgO Films on a Mo(100) Surface Studied by Infrared Reflection–Absorption Spectroscopy, Temperature Programmed Desorption, and X-ray Photoelectron Spectroscopy. *J. Vac. Sci. Technol. A* **1992**, *10*, 2248–2252. [[CrossRef](#)]
25. Huang, Y.; Ong, C.W.; Yeo, B.S. Effects of Electrolyte Anions on the Reduction of Carbon Dioxide to Ethylene and Ethanol on Copper (100) and (111) Surfaces. *ChemSusChem* **2018**, *11*, 3299–3306. [[CrossRef](#)] [[PubMed](#)]

26. Peterson, A.A.; Abild-Pedersen, F.; Studt, F.; Rossmeisl, J.; Nørskov, J.K. How Copper Catalyzes the Electroreduction of Carbon Dioxide into Hydrocarbon Fuels. *Energy Environ. Sci.* **2010**, *3*, 1311–1315. [[CrossRef](#)]
27. Hori, Y.; Murata, A.; Takahashi, R. Formation of Hydrocarbons in the Electrochemical Reduction of Carbon Dioxide at a Copper Electrode in Aqueous Solution. *J. Chem. Soc. Faraday Trans. 1* **1989**, *85*, 2309–2326. [[CrossRef](#)]
28. Gao, D.; Scholten, F.; Roldan Cuenya, B. Improved CO₂ Electroreduction Performance on Plasma-Activated Cu Catalysts via Electrolyte Design: Halide Effect. *ACS Catal.* **2017**, *7*, 5112–5120. [[CrossRef](#)]
29. Dutta, A.; Rahaman, M.; Mohos, M.; Zanetti, A.; Broekmann, P. Electrochemical CO₂ conversion using skeleton (sponge) type of Cu catalysts. *ACS Catal.* **2017**, *7*, 5431–5437. [[CrossRef](#)]
30. Dutta, A.; Rahaman, M.; Luedi, N.C.; Mohos, M.; Broekmann, P. Morphology matters: Tuning the product distribution of CO₂ electroreduction on oxide-derived Cu foam catalysts. *ACS Catal.* **2016**, *6*, 3804–3814. [[CrossRef](#)]
31. Tang, W.; Peterson, A.A.; Varela, A.S.; Jovanov, Z.P.; Bech, L.; Durand, W.J.; Dahl, S.; Nørskov, J.K.; Chorkendorff, I. The importance of surface morphology in controlling the selectivity of polycrystalline copper for CO₂ electroreduction. *Phys. Chem. Chem. Phys.* **2012**, *14*, 76–81. [[CrossRef](#)] [[PubMed](#)]
32. Mariano, R.G.; McKelvey, K.; White, H.S.; Kanan, M.W. Selective increase in CO₂ electroreduction activity at grain-boundary surface terminations. *Science* **2017**, *358*, 1187–1192. [[CrossRef](#)] [[PubMed](#)]
33. Gupta, N.; Gattrell, M.; MacDougall, B. Calculation for the cathode surface concentrations in the electrochemical reduction of CO₂ in KHCO₃ solutions. *J. Appl. Electrochem.* **2006**, *36*, 161–172. [[CrossRef](#)]
34. Zhang, K.; Zhang, G.; Liu, X.; Phan, A.N.; Luo, K. A Study on CO₂ Decomposition to CO and O₂ by the Combination of Catalysis and Dielectric-Barrier Discharges at Low Temperatures and Ambient Pressure. *Ind. Eng. Chem. Res.* **2017**, *56*, 3204–3216. [[CrossRef](#)]
35. Dutta, A.; Montiel, I.Z.; Erni, R.; Kiran, K.; Rahaman, M.; Drnec, J.; Broekmann, P. Activation of Bimetallic AgCu Foam Electrocatalysts for Ethanol Formation from CO₂ by Selective Cu Oxidation/Reduction. *Nano Energy* **2020**, *68*, 104331. [[CrossRef](#)]
36. Dutta, A.; Rahaman, M.; Hecker, B.; Drnec, J.; Kiran, K.; Montiel, I.Z.; Weber, D.J.; Zanetti, A.; López, A.C.; Martens, I.; et al. CO₂ electrolysis—Complementary *operando* XRD, XAS and Raman spectroscopy study on the stability of Cu_xO foam catalysts. *J. Catal.* **2020**, *389*, 592–603. [[CrossRef](#)]
37. Hanselman, S.; Koper, M.T.; Calle-Vallejo, F. Computational comparison of late transition metal (100) surfaces for the electrocatalytic reduction of CO to C₂ species. *ACS Energy Lett.* **2018**, *3*, 1062–1067. [[CrossRef](#)]
38. Dutta, A.; Morstein, C.E.; Rahaman, M.; Lopez, A.C.; Broekmann, P. Beyond Copper in CO₂ Electrolysis: Effective Hydrocarbon Production on Silver-Nanofoam Catalysts. *ACS Catal.* **2018**, *8*, 8357–8368. [[CrossRef](#)]
39. Reller, C.; Krause, R.; Volkova, E.; Schmid, B.; Neubauer, S.; Rucki, A.; Schuster, M.; Schmid, G. Selective Electroreduction of CO₂ toward Ethylene on Nano Dendritic Copper Catalysts at High Current Density. *Adv. Energy Mater.* **2017**, *7*, 1602114. [[CrossRef](#)]
40. Padilla, M.; Baturina, O.; Gordon, J.P.; Artyushkova, K.; Atanassov, P.; Serov, A. Selective CO₂ electroreduction to C₂H₄ on porous Cu films synthesized by sacrificial support method. *J. CO₂ Util.* **2017**, *19*, 137–145. [[CrossRef](#)]
41. Hoang, T.T.H.; Verma, S.; Ma, S.; Fister, T.T.; Timoshenko, J.; Frenkel, A.I.; Kenis, P.J.A.; Gewirth, A.A. Nanoporous Copper–Silver Alloys by Additive-Controlled Electrodeposition for the Selective Electroreduction of CO₂ to Ethylene and Ethanol. *J. Am. Chem. Soc.* **2018**, *140*, 5791–5797. [[CrossRef](#)] [[PubMed](#)]
42. Ahn, S.; Klyukin, K.; Wakeham, R.J.; Rudd, J.A.; Lewis, A.R.; Alexander, S.; Carla, F.; Alexandrov, V.; Andreoli, E. Poly-Amide Modified Cu foam Electrodes for Enhanced Electrochemical Reduction of Carbon Dioxide. *ACS Catal.* **2018**, *8*, 4132–4142. [[CrossRef](#)]
43. Hoang, T.T.; Ma, S.; Gold, J.I.; Kenis, P.J.; Gewirth, A.A. Nanoporous copper films by additive-controlled electrodeposition: CO₂ reduction catalysis. *ACS Catal.* **2017**, *7*, 3313–3321. [[CrossRef](#)]
44. Dunwell, M.; Lu, Q.; Heyes, J.M.; Rosen, J.; Chen, J.G.; Yan, Y.; Jiao, F.; Xu, B. The Central Role of Bicarbonate in the Electrochemical Reduction of Carbon Dioxide on Gold. *J. Am. Chem. Soc.* **2017**, *139*, 3774–3783. [[CrossRef](#)]

Disclaimer/Publisher’s Note: The statements, opinions and data contained in all publications are solely those of the individual author(s) and contributor(s) and not of MDPI and/or the editor(s). MDPI and/or the editor(s) disclaim responsibility for any injury to people or property resulting from any ideas, methods, instructions or products referred to in the content.